Evolution of Melt Pond Fraction and Depth on Multiyear Ice in 2020 from High Resolution Satellite Observations

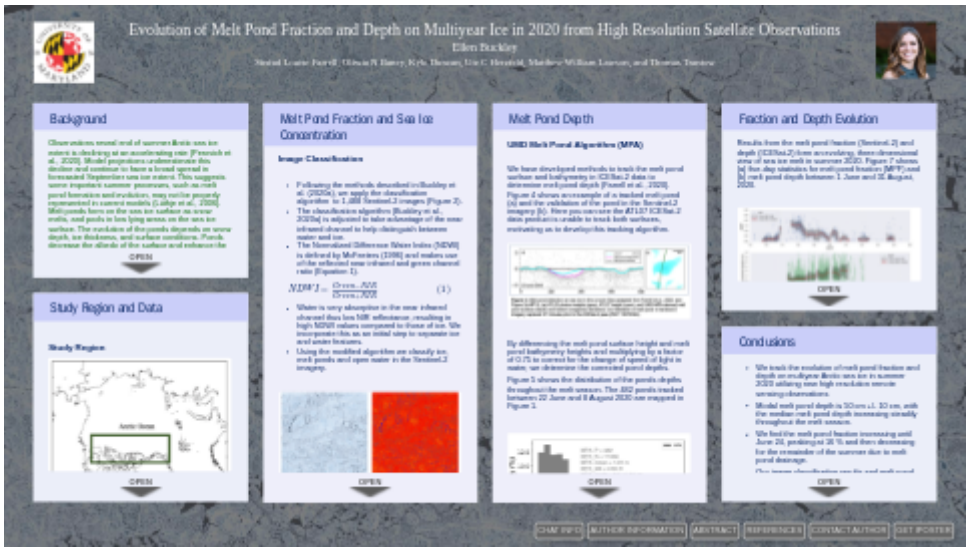

Ellen Buckley

Sinéad Louise Farrell, Oliwia N Baney, Kyle Duncan, Ute C Herzfeld, Matthew William Lawson, and Thomas Trantow

PRESENTED AT:

BACKGROUND

Observations reveal end of summer Arctic sea ice extent is declining at an accelerating rate (Perovich et al., 2020). Model projections underestimate this decline and continue to have a broad spread in forecasted September sea ice extent. This suggests some important summer processes, such as melt pond formation and evolution, may not be properly represented in current models (Lüthje et al., 2006). Melt ponds form on the sea ice surface as snow melts, and pools in low lying areas on the sea ice surface. The evolution of the ponds depends on snow depth, ice thickness, and surface conditions. Ponds decrease the albedo of the surface and enhance the positive ice albedo feedback, accelerating further melt (Perovich and Polashenski, 2012).

The influence of melt ponds on the evolution of summer sea ice melt shown by models, drives our work to understand the evolution of ponds on the ice. Is our existing knowledge of melt ponds on sea ice still representative of the “new Arctic?” Do the relationships between melt pond fraction and melt pond depth observed over twenty years ago (Perovich et al., 2002), that inform melt pond parameterizations in sea ice models still persist?

ICESat-2, launched in 2018, is the first photon counting satellite laser altimeter, and provides high resolution details of melt pond bathymetry. Sentinel-2, launched in 2015 (A) and 2017 (B), provides high resolution visible and near-infrared imagery, and here, is used to validate the melt ponds identified in ICESat-2, as well as provide additional information about the evolving sea ice surface.

We derive parameters from Sentinel-2 and ICESat-2 remote sensing observations that describe the evolution of melt on multiyear sea ice in summer. We examine melt pond depth and fraction and explore the relationships between these melt pond characteristics.

STUDY REGION AND DATA

Study Region

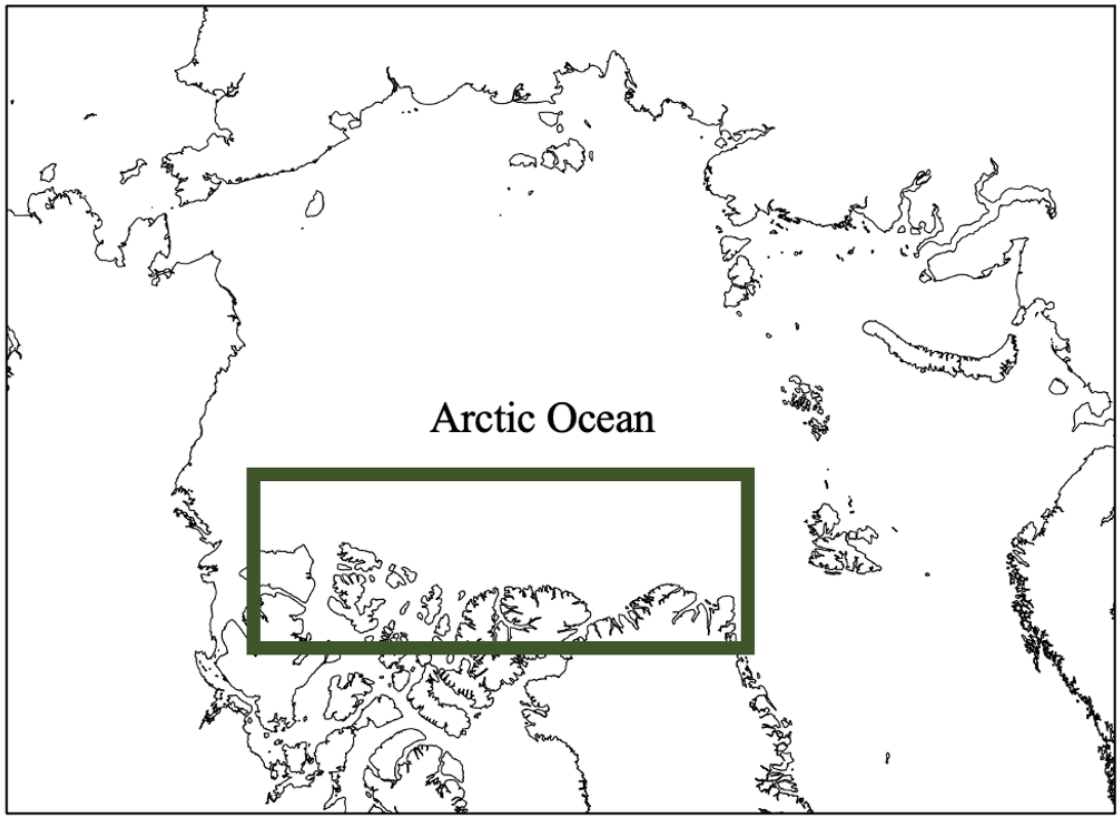

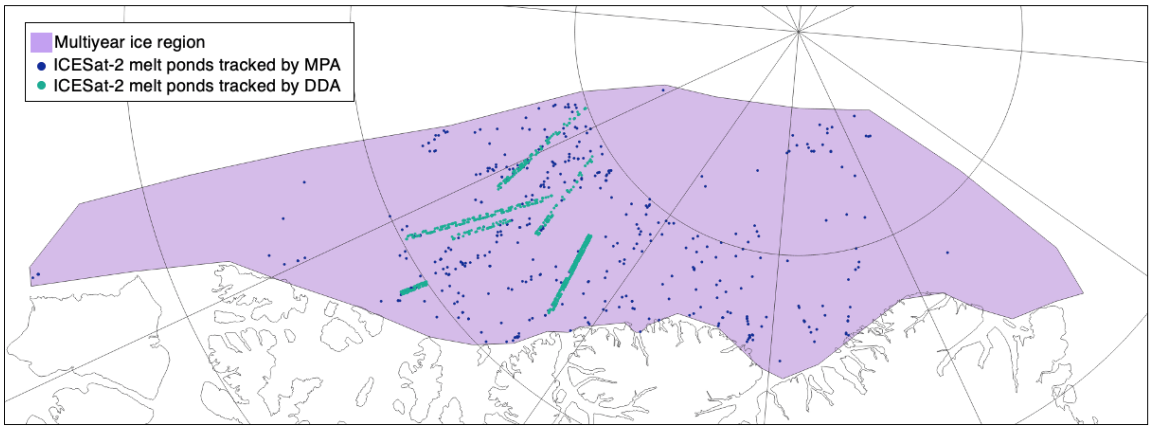

Figure 1. Study region. The 2020 multiyear ice region show in purple, locations of the ICESat-2 melt ponds tracked by the MPA (navy) and locations of ICESat-2 melt ponds tracked by the DDA (aqua).

Multiyear ice is thicker and contains less brine than younger ice, so it is more difficult for icebreakers to navigate through. However, these characteristics make it a more reliable mode of transportation for indigenous populations to hunt and fish. With the extent and thickness of multiyear ice diminishing at an alarming rate, we must understand the processes that contribute to the summer melt. The extent of the multiyear ice region was estimated using the MetOp Sea Ice NOAA Ice Mode Mask and sea ice type product of the EUMETSAT Ocean and Sea Ice Satellite Application Facility (OSI SAF, osi-saf.eumetsat.int) on 15 May 2020, prior to melt onset (Figure 1).

This region hosts the oldest and thickest ice in the Arctic, and was chosen for the study region as the thick ice can hold melt ponds for a longer period of time without melting through the ice pack as compared to thinner first year ice. The ability to measure melt pond depth on multiyear ice with satellite altimetry was first shown in Farrell et al., 2020. There we demonstrate 339 depths retrievals from 15 ponds and found depths ranging from 0.04 - 2.4 m with a modal depth of 0.35 m. In Buckley et al., 2020b, we discussed continued work to track ponds and introduced the DDA- bifurcate (Herzfeld et al., 2017), an additional algorithm to track ponds in ICESat-2 data. The work presented here continues to build on these efforts to create a melt pond database.

Data

In this study, we examine ICESat-2 and Sentinel-2 data from 1 June 2020 through 31 August 2020 in this region to capture the full melt season.

ICESat-2, a photon counting laser altimeter launched in 2018, provides high resolution detail of sea ice and snow topography due to its unique combination of a small footprint (~12 m) and high-resolution along-track sampling (0.7 m) (Markus et al., 2017). The green laser (532 nm) is able to penetrate water, enabling melt pond depth measurements (Farrell et al., 2020). ICESat-2 data are available here (https://nsidc.org/data/icesat-2/data-sets).

The Sentinel-2 satellites (A and B) have a 98° inclination and coverage of all coastal waters up to 20 km from the shore, up to 84° N. Sentinel-2 imagery is widely available throughout the multiyear ice region due to the proximity to land. The Level 1C Top of Atmosphere Reflectances are provided in 13 spectral bands ranging from visible (490 – 665 nm) to short wave infrared (2190 nm) (Drusch et al., 2012). We utilize the 10 m resolution visible and near infrared bands (B02 (centered at 490 nm), B03 (560 nm), B04 (665 nm), and B08 (842 nm)) in this work. Sentinel-2 data were retrieved from here. (https://apps.sentinel-hub.com/)

MELT POND FRACTION AND SEA ICE CONCENTRATION

Image Classification

- Following the methods described in Buckley et al. (2020a), we apply the classification algorithm to 1,488 Sentinel-2 images (Figure 2).
- The classification algorithm (Buckley et al., 2020a) is adjusted to take advantage of the near infrared channel to help distinguish between water and ice.
- The Normalized Difference Water Index (NDWI) is defined by McFeeters (1996) and makes use of the reflected near infrared and green channel ratio (Equation 1).

$$NDWI = \frac{Green - NIR}{Green + NIR} \qquad (1)$$

- Water is very absorptive in the near infrared channel thus low NIR reflectance, resulting in high NDWI values compared to those of ice. We incorporate this as an initial step to separate ice and water features.
- Using the modified algorithm we classify ice, melt ponds and open water in the Sentinel-2 imagery.

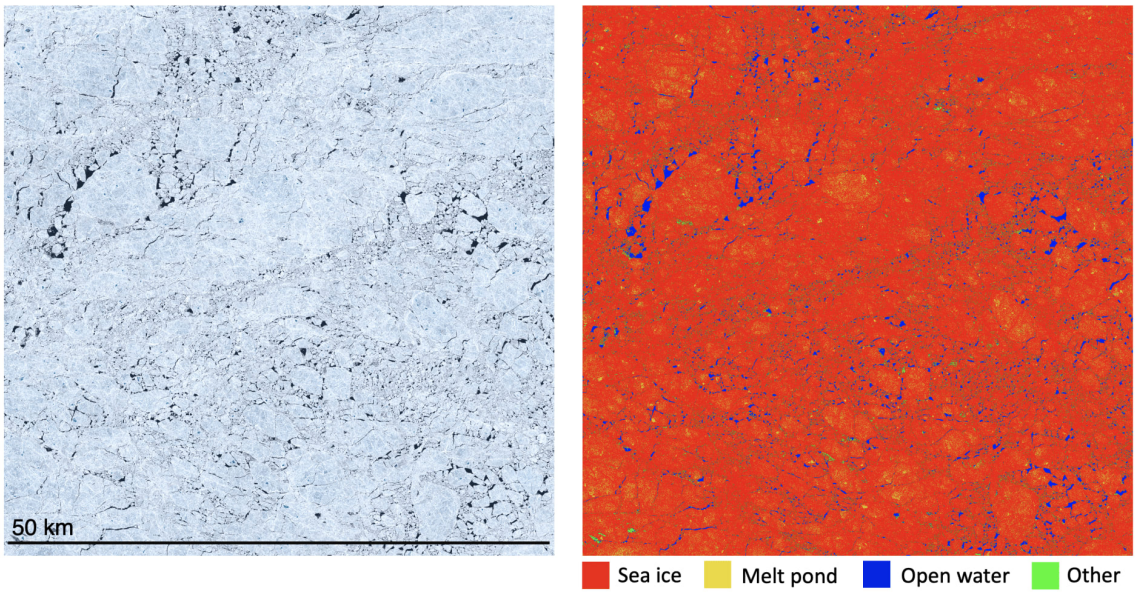

Figure 2. Classification of Sentinel-2 imagery at -114.0° W, 80.5° N on 21 July, 2020. Image on the left is the Sentinel-2 true color imagery. Image on the right shows the classification of sea ice (red), melt ponds (yellow), open water (blue), and other (green).

From the classified pixels, we are able to calculate melt pond fraction (MPF) and sea ice concentration (SIC). MPF is defined as the fraction of the sea ice covered in melt ponds. SIC is the fraction of the ocean covered in sea ice. In the Sentinel-2 examples shown in Figure 2, MPF is estimated at 11.5% while SIC is 96.4%.

Classification Validation

We validate the Sentinel-2 classification with higher resolution (1.45 m) WorldView imagery (Figure 3). Processed WorldView-2 data were provided to this project by the Polar Geospatial Center under NSF and NASA Cryosphere Program support.

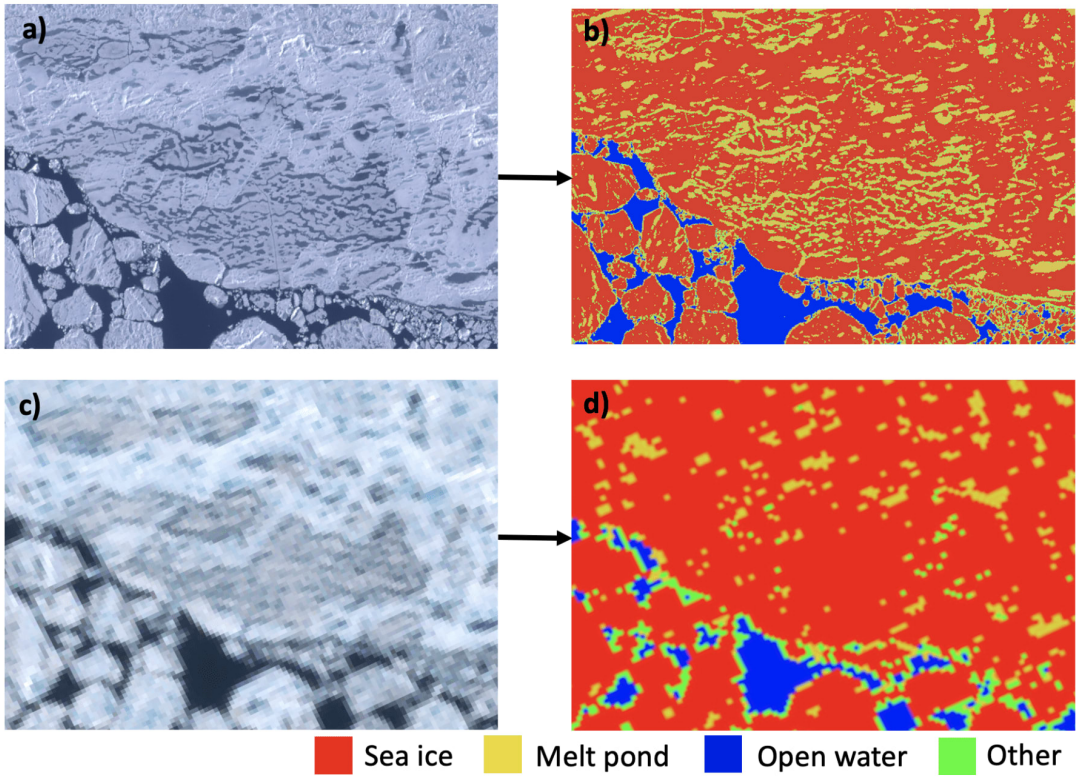

Figure 3. A 1 km x 0.8 m image of coincident Worldview-2 (a) and Sentinel-2 (c) imagery and the classified image. Classification of these images (b and d, respectively) shows sea ice (red), melt pond (yellow), open water (blue) and other (green). The image is located at (-110° W , 80° N) and was observed on 27 July, 2020 (DOY 209).

Small features on sea ice pose a challenge for satellite-derived classification. Given ponds can range in size from 10s to 100s of meters in diameter, it is challenging to fully account for MPF in the 10 m resolution Sentinel-2 data. Assessing coincident data from the higher-resolution (1.45 m) WorldView-2 imagery we find that MPF can be biased low in the S2 results when small ponds are widespread across the surface. For example, in Fig 3, we estimate MPFs of 7.6 % and 25.5 % from S2 and WV, respectively. Similarly, we find that SIC is biased higher in the lower resolution iamgery.
We estimate SIC as 93.5% and 87.3% from Sentinel-2 and WorldView imagery, respectively. These results are consistent with previous findings, Buckley et al. (2020a) and refs. therein.

MELT POND DEPTH

UMD Melt Pond Algorithm (MPA)

We have developed methods to track the melt pond surface and bathymetry in ICESat-2 data to determine melt pond depth (Farrell et al., 2020). Figure 4 shows an example of a tracked melt pond (a) and the validation of the pond in the Sentinel-2 imagery (b). Here you can see the ATL07 ICESat-2 data product is unable to track both surfaces, motivating us to develop this tracking algorithm.

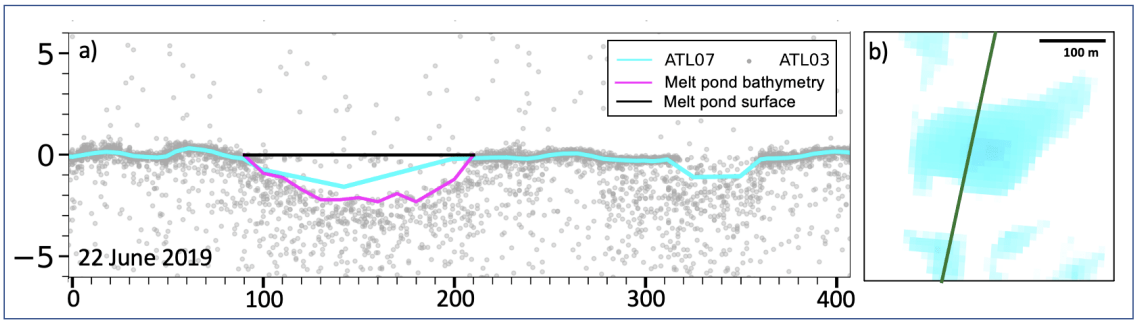

Figure 4. Melt pond detection on sea ice in the Lincoln Sea (adapted from Farrell et al., 2020, see Figure 2a MP 9). (a) ATL03 photon heights (gray), ATL07 height (cyan), and UMD-MPA-derived melt pond surface (black) and bottom (magenta) elevations. (b) Validation of melt pond in Sentinel-2 imagery captured 37 minutes prior to the ICESat-2 pass (RGT 13070304).

By differencing the melt pond surface height and melt pond bathymetry heights and multiplying by a factor of 0.75 to correct for the change of speed of light in water, we determine the corrected pond depths.

Figure 5 shows the distribution of the ponds depths throughout the melt season. The 482 ponds tracked between 22 June and 8 August 2020 are mapped in Figure 1.

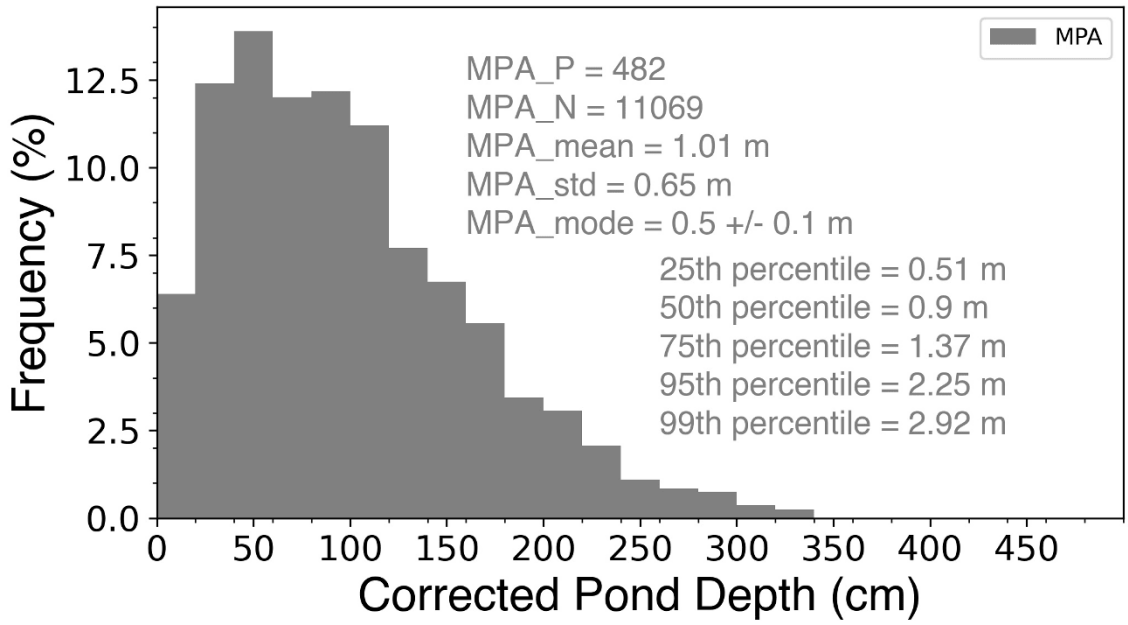

Figure 5. Distribution of corrected melt pond depths derived from the UMD-MPA.

Figure 5 shows there are over 11,000 depth measurements from 482 melt ponds in 103 ICESat-2 tracks . The median melt pond depth is 90 cm and modal depth is 50 cm. The mean, mode, and median from this dataset are are all approximately 0.15 m greater than reported in Farrell et al., (2020) for the 15 ponds tracked in 2019. This can be explained by the temporal range of melt ponds in this study extending through July and into August, whereas the Farrell et al., (2020) study only includes ponds from mide to late June. We show in Figure 7, mean melt pond depths increase throughout the melt season.

CU Density Dimension Algorithm - Bifurcate (DDA)

- DDA builds on a calculation of the density field as a form of data aggregation (Herzfeld et al., 2017).
- DDA-Bifurcate automatically detects whether there are two surfaces or one
- Detection of ponds is carried out by the DDA (Figure 6).
- The DDA-Bifurcate algorithm is adaptive and fully automated such that pond locations do not need to be provided a priori to the algorithm.

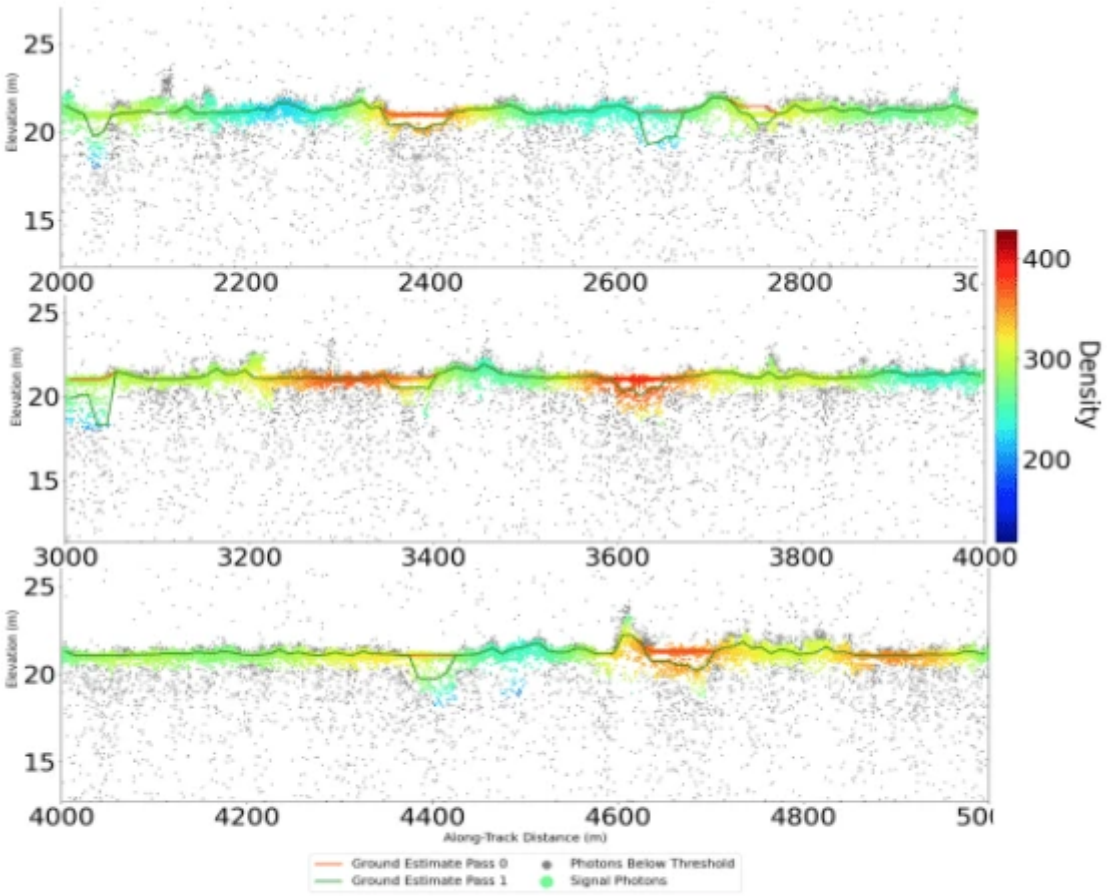

Figure 6. Example DDA tracking of ICESat-2 ATL03 surfaces. The first pass is shown in red, and the second surface in green.

Here we test the DDA-Bifurcate algorithm on five ICESat-2 orbit segments that transect our study region. Based on a visual inspection of ICESat-2 ATL03 data, these tracks were selected for study due to the presence of widespread surface ponding. In a 70 km section, the DDA-Bifurcate finds approximately 50 ponds per strong beam, where the MPA only find 11 ponds. This demonstrates the necessity of an adaptive and automated approach to fully capture pond conditions on the sea ice during melt. Future work includes applying the DDA-algorithm to all cloud-free orbit segments crossing the study region to estimate pond depth evolution between 1 June and 31 August 2020. Results from the MPA will be used to evaluate DDA-Bifurcate results.

FRACTION AND DEPTH EVOLUTION

Results from the melt pond fraction (Sentinel-2) and depth (ICESat-2) form an evolving, three dimensional view of sea ice melt in summer 2020. Figure 7 shows (a) five-day statistics for melt pond fraction (MPF) and (b) melt pond depth between 1 June and 31 August, 2020.

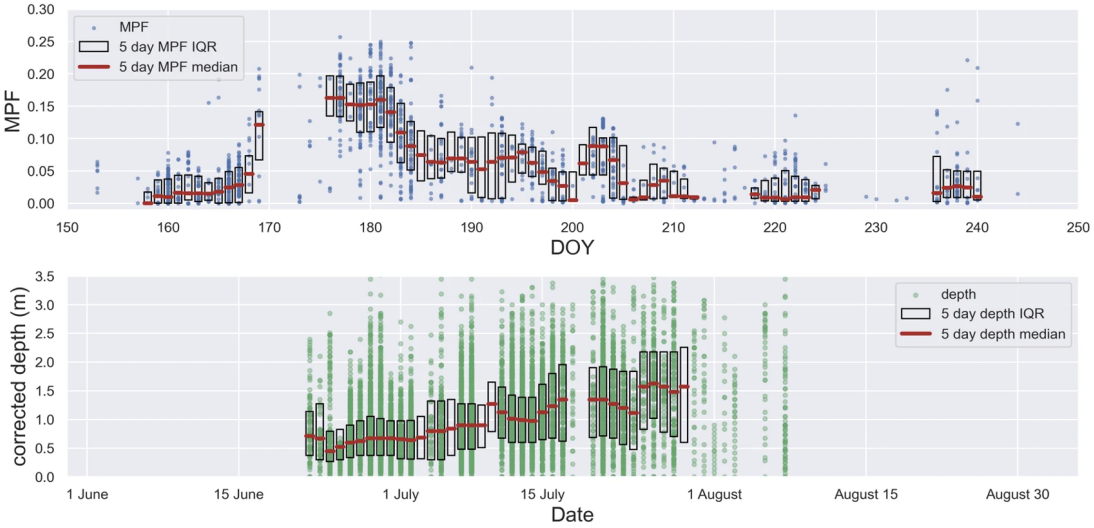

Figure 7. Seasonal evolution of melt pond parameters on multiyear ice in the 2020 melt season. (a) Melt pond fraction derived from Sentinel-2 and (b) depth derived the the MPA results. Five day running means are shown as a horizontal red line, 5 day means as a black dot, and the interquartile range denoted by the box.

MPF across the MYI ice region, calculated from 1,477 Sentinel-2 images, averaged 6.5% with a standard deviation of 6.5%. The highest MPF for an individual Sentinel-2 scene was 31.6%. This image is located just outside of the mouth of Nansen Sound at (-95.3° W, 82.3° N), but far enough from that coastline that it does not include landfast ice. The evolution of MPF is shown in Figure 7a. The five day median for periods with greater than 15 images is shown as the red horizontal line. MPF remains low, <5%, through 16 June (DOY 168). We then see a sharp increase in the five day running mean on 17 June (DOY 169). The imagery is scarce between 18 and 22 June due to widespread cloud coverage. This weather system likely enhances the melt and when it passes we see high MPF 24-29 June. The peak five day median MPF is 16.0% on 24 June.

Similarly, Figure 7b shows the melt pond depth evolution. There are over 11,000 individual measurements of pond depth represented by the green dots. The 5 day running mean statistics are represented by the red line (median) and the box (IQR). Melt pond depth increases throughout the summer season. This is consistent with Scott and Feltham (2010) showing rapid pond deepening on multiyear ice. The median depth is 0.9 m and the mean is 1.0 m with a standard deviation of 0.65 m. For more statistics on the pond depth results see Figure 5. The melt pond depth evolution is not representative of a single pond, as ponds have complex meltwater accumulation and vertical and lateral drainage processes. Freeze onset in August causes the ponds to form ice lids resulting in a pond depth measurement of zero, although there may be liquid water beneath the ice lid. Freeze conditions occur at different points in this region at the end of summer, as you can see fewer pond depth measurements throughout the month of August.

Figure 8 shows sections of WorldView images and classifications demonstrating the phases of melt pond evolution.

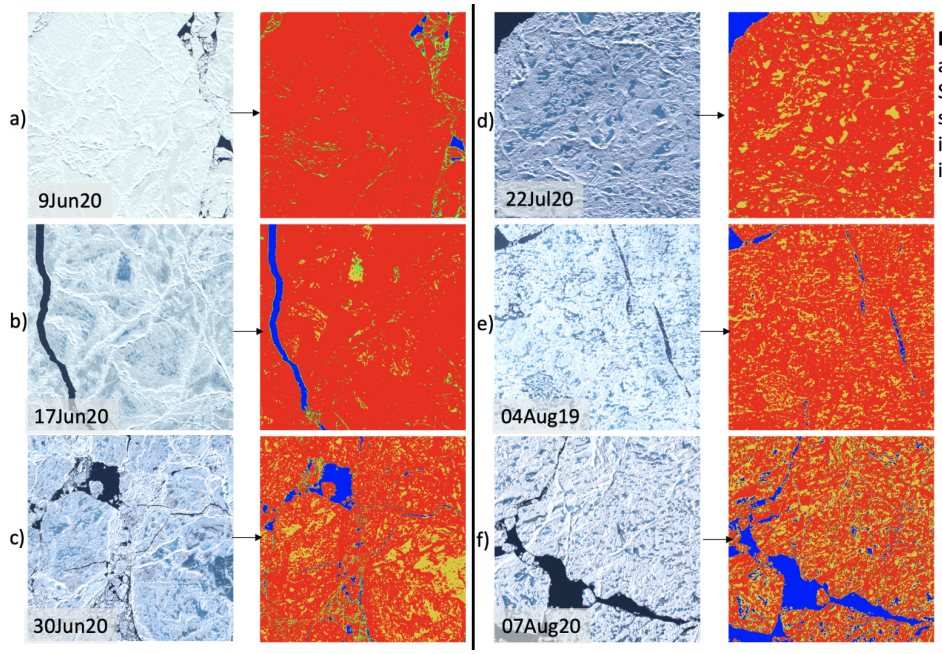

Figure 8. Melt evolution across the MYI region in Summer 2020, based on a selection of Worldview imagery (~ 900m x 900 m in area).

	MPF	SIC
a)	<1%	99%
b)	2.8%	97%
c)	22.8%	95.9%
d)	14.5%	98.2%
e)	18.9%	98.6%
f)	31.9%	85.5%

Figure 8a, on 9 June 2020, while the surface may be undergoing melt and snow metamorphism is taking place, no ponds are detected in surface imagery. In b) on 17 June 2020, ponds have formed and the meltwater has pooled into the lowest topographic areas. In c) on 30 June 2020, melt has advanced with a higher fraction of the ice covered in ponds. Image d) on 22 July 2020, shows drainage channels that have formed between ponds as ponds drain into other ponds and into the open ocean, either laterally of vertically. Figure e) on 4 August 2019 shows regions of the ice have melted through, exposing the ocean, and pockets of open water have formed within the floe. In f) on 7 August 2020, ice lids have begun to form on the pond surface. Still, a large fraction of the ice is covered in ponds.

CONCLUSIONS

- We track the evolution of melt pond fraction and depth on multiyear Arctic sea ice in summer 2020 utilizing new high resolution remote sensing observations
- Modal melt pond depth is 50 cm +/- 10 cm, with the median melt pond depth increasing steadily throughout the melt season.
- We find the melt pond fraction increasing until June 24, peaking at 16 % and then decreasing for the remainder of the summer due to melt pond drainage.
- Our image classification results and melt pond depth products may be of interest to those studying under-ice light and biology, as well as modelers who are interested in understanding the evolution of melt pond parameters for model initialization and validation.
- We have demonstrated that the vertical resolution of the ATLAS data from ICESat-2 are sufficient to resolve ponds on multiyear ice. Due to surface topography and snow cover, these ponds tend to be discrete deep ponds that pool across the surface. Shallower, more extensive ponding on FYI presents a challenge since the minimum vertical resolution of the current methodology is 10 cm. Future work includes evaluating the performance of existing algorithms across a broader range of ice types.

Future work

- Apply DDA algorithm to all summer 2020 MYI region tracks.
- Test feasibility of tracking ponds on other ice types
- Expand the melt pond database by tracking ponds in other regions and years.
- Compare melt pond statistics with 2020 in situ and airborne measurements conducted as part of the MOSAiC campaign (Shupe et al., 2020).
- Work towards a unified melt pond depth recovery algorithm for automatic application to ICESat-2 data.

Acknowledgements

This study is supported under NASA Cryosphere Program Grant 80NSSC17K0006 (PI Sinead Farrell) and NASA Earth Sciences Award 80NSSC20K0975 (PI Ute Herzfeld)

Geospatial support for this work provided by the Polar Geospatial Center under NSF-OPP awards 1043681 and 1559691.

AUTHOR INFORMATION

Ellen Buckley[1], Sinéad Louise Farrell[1], Oliwia N Baney[1], Kyle Duncan[2], Ute C Herzfeld[3] , Matthew William Lawson[4], and Tom Trantow[3]

1. University of Maryland College Park, College Park, MD, United States,

2. University of Maryland, Earth System Science Interdisciplinary Center, College Park, MD, United States,

3. Univ Colorado Boulder, Electrical, Computer and Energy Engineering and CIRES, Boulder, CO, United States

4. University of Colorado Boulder, Computer Science, Boulder, CO, United States

ABSTRACT

Observations reveal end of summer Arctic sea ice extent is declining at an accelerating rate. Model projections underestimate this decline and continue to have a broad spread in forecasted September sea ice extent. This suggests some important summer processes, such as melt pond formation and evolution, may not be properly represented in current models. Melt ponds form on the sea ice surface as snow melts, and pools in low lying areas on the sea ice surface. The evolution of the ponds depends on snow depth, ice thickness, and surface conditions. Melt water may spread across a level surface, or be confined to depressions between sea ice ridges. Ponds decrease the albedo of the surface and enhance the positive ice albedo feedback, accelerating further melt. Until recently, Arctic-wide observations of individual melt ponds were not available. ICESat-2, a photon counting laser altimeter launched in 2018, provides high resolution detail of sea ice and snow topography due to its unique combination of a small footprint (~12 m) and high-resolution along-track sampling (0.7 m). The green laser (532 nm) is able to penetrate water, enabling melt pond depth measurements. We have developed methods to track the melt pond surface and bathymetry in ICESat-2 data to determine melt pond depth. We also track melt pond evolution through application of a sea ice classification algorithm to 10 m resolution Sentinel-2 imagery. The combination of these two datasets allows for an evolving, three-dimensional view of the melting sea ice surface. We focus on the evolution of summer melt on multiyear ice in the Central Arctic north of Greenland and Canada in 2020. Our findings are put in context of existing literature on melt pond depth, volume, and evolution. We also discuss our results in relation to the melt pond fraction north of the Fram Strait, where we expect different ice conditions in the vicinity of the 2020 MOSAiC field studies. Observational data products comprising melt pond fraction and pond depth are being developed for public distribution. These products may be of interest to those studying under-ice light and biology, as well as modelers who are interested in understanding the evolution of melt pond parameters for model initialization and validation.

REFERENCES

Buckley, E. M., Farrell, S. L., Duncan, K., Connor, L. N., Kuhn, J. M., & Dominguez, R. T. (2020a). Classification of sea ice summer melt features in high-resolution IceBridge imagery. Journal of Geophysical Research: Oceans, 125, e2019JC015738. https://doi.org/10.1029/2019JC015738 (https://doi.org/10.1029/2019JC015738)

Buckley, E., Farrell, S. L., Duncan, K., & Herzfeld, U. C. (2020b, December). ICESat-2 observations of melt ponds on Arctic sea ice. In AGU Fall Meeting Abstracts (Vol. 2020, pp. C017-01). https://(https://doi.org/10.1029/2020GL090708)doi.org/10.1002/essoar.10508493.1 (https://doi.org/10.1002/essoar.10508493.1)

Drusch, M., Del Bello, U., Carlier, S., Colin, O., Fernandez, V., Gascon, F., … Bargellini, P. (2012). Sentinel-2: ESA's Optical High-Resolution Mission for GMES Operational Services. Remote Sensing of Environment, 120, 25–36. https://doi.org/10.1016/j.rse.2011.11.026 (https://doi.org/10.1016/j.rse.2011.11.026)

Farrell, S. L., Duncan, K., Buckley, E. M., Richter-Menge, J., & Li, R. (2020). Mapping sea ice surface topography in high fidelity with ICESat-2. Geophysical Research Letters, 47, e2020GL090708. https://doi.org/10.1029/2020GL090708 (https://doi.org/10.1029/2020GL090708)

Herzfeld, U. C., Trantow, T. M., Harding, D., & Dabney, P. W. (2017). Surface-height determination of crevassed glaciers—Mathematical principles of an autoadaptive density-dimension algorithm and validation using ICESat-2 simulator (SIMPL) data. IEEE Transactions on Geoscience and Remote Sensing, 55(4), 1874-1896.

Herzfeld, U. C., Trantow, T., Lawson, M., Hans, J., & Medley, G. (2021). Surface heights and crevasse morphologies of surging and fast-moving glaciers from ICESat-2 laser altimeter data-Application of the density-dimension algorithm (DDA-ice) and evaluation using airborne altimeter and Planet SkySat data. Science of Remote Sensing, 3, 100013.

Lüthje, M., Feltham, D. L., Taylor, P. D., & Worster, M. G. (2006). Modeling the summertime evolution of sea−ice melt ponds. Journal of Geophysical Research: Oceans, 111(C2).

Markus, T., Neumann, T., Martino, A., Abdalati, W., Brunt, K., Csatho, B., … Zwally, J. (2017). The Ice, Cloud, and land Elevation Satellite-2 (ICESat-2): Science requirements, concept, and implementation. Remote Sensing of Environment, 190, 260-273. https://doi.org/10.1016/j.rse.2016.12.029 (https://doi.org/10.1016/j.rse.2016.12.029)

Perovich, D. K., Tucker III, W. B., & Ligett, K. A. (2002). Aerial observations of the evolution of ice surface conditions during summer. Journal of Geophysical Research: Oceans, 107(C10), SHE-24.

Perovich, D. K., Meier, W., Tschudi, M., Hendricks, S., Petty, A. A., Divine, D., Farrell, S., Gerland, S., Haas, C., Kaleschke, L., Pavlova, O., Ricker, R., Tian-Kunze, X., Webster, M., & Wood, K. (2020). Sea Ice [in Arctic Report Card 2020]. Arctic Report Card 2020.

Scott, F., & Feltham, D. L. (2010). A model of the three−dimensional evolution of Arctic melt ponds on first−year and multiyear sea ice. Journal of Geophysical Research: Oceans, 115(C12).

Shupe, M. D., Rex, M., Dethloff, K., Damm, E., Fong, A. A., Gradinger, R., ... & Sommerfeld, A. (2020). The MOSAiC Expedition: A Year Drifting with the Arctic Sea Ice. Arctic report card.